Atmos. Chem. Phys. Discuss., 14, 8779–8818, 2014
www.atmos-chem-phys-discuss.net/14/8779/2014/
doi:10.5194/acpd-14-8779-2014

Atmospheric Chemistry and Physics
Discussions
Open Access

This discussion paper is/has been under review for the journal Atmospheric Chemistry and Physics (ACP). Please refer to the corresponding final paper in ACP if available.

Aerosol radiative effects in the ultraviolet, visible, and near-infrared spectral ranges using long-term aerosol data series over the Iberian Peninsula

D. Mateos[1,2], M. Antón[1], C. Toledano[2], V. E. Cachorro[2], L. Alados-Arboledas[3,4], M. Sorribas[3,4,5], M. J. Costa[6], and J. M. Baldasano[7]

[1]Departamento de Física, Universidad de Extremadura, Badajoz, Spain
[2]Grupo de Óptica Atmosférica, Universidad de Valladolid, Paseo Belén 7, 47011, Valladolid, Spain
[3]Departamento de Física Aplicada, Universidad de Granada, Granada, Spain
[4]Andalusian Institute for Earth System Research, Universidad de Granada, Granada, Spain
[5]Estación de Sondeos Atmosféricos El Arenosillo, INTA, Huelva, Spain
[6]Évora Geophysics Centre and Dep. Physics, University of Évora, Évora, Portugal
[7]Universidad Politécnica de Cataluña, Barcelona, Spain

Received: 14 February 2014 – Accepted: 22 March 2014 – Published: 2 April 2014

Correspondence to: D. Mateos (mateos@goa.uva.es)

Published by Copernicus Publications on behalf of the European Geosciences Union.

Abstract

A better understanding of the aerosol radiative properties is a crucial challenge for climate change studies. This study aims to provide a complete characterization of aerosol radiative effects in different spectral ranges within the shortwave (SW) solar spectrum. For this purpose, long-term datasets of aerosol properties from six AERONET stations located in the Iberian Peninsula (Southwestern Europe) are analyzed in term of climatology characterization and trends. Aerosol information is used as input to the libRadtran model in order to determine the aerosol radiative effect at the surface in the ultraviolet (ARE_{UV}), visible (ARE_{VIS}), near-infrared (ARE_{NIR}), and the entire SW range (ARE_{SW}) under cloud-free conditions. Over the whole Iberian Peninsula, aerosol radiative effects in the different spectral ranges are: $-1.1 < ARE_{UV} < -0.7\,W\,m^{-2}$, $-5.7 < ARE_{VIS} < -3.8\,W\,m^{-2}$, $-2.8 < ARE_{NIR} < -1.7\,W\,m^{-2}$, and $-9.5 < ARE_{SW} < -6.1\,W\,m^{-2}$. The four variables showed positive statistically significant trends between 2004 and 2012, e.g., ARE_{SW} increased $+3.6\,W\,m^{-2}$ per decade. This fact is linked to the decrease in the aerosol load, which presents a trend of −0.04 per unit of aerosol optical depth at 500 nm per decade, hence a reduction of aerosol effect on solar radiation at the surface is seen. Monthly means of ARE show a seasonal pattern with larger values in spring and summer. The aerosol forcing efficiency (AFE), ARE per unit of aerosol optical depth, is also evaluated in the four spectral ranges. AFE exhibits a dependence on single scattering albedo and a weaker one on Ångström exponent. AFE is larger (in absolute value) for small and absorbing particles. The contributions of the UV, VIS, and NIR ranges to the SW efficiency vary with the aerosol types. Aerosol size determines the fractions of AFE_{VIS}/AFE_{SW} and AFE_{NIR}/AFE_{SW}. VIS range is the dominant region for all types, although non-absorbing large particles cause a more equal contribution of VIS and NIR intervals. The AFE_{UV}/AFE_{SW} ratio shows a higher contribution for absorbing fine particles.

ACPD
14, 8779–8818, 2014

1 Introduction

Atmospheric aerosol particles can absorb and scatter part of the total amount of solar radiation entering the Earth's atmosphere. In fact, aerosols directly influence the Earth's energy budget and act as cloud condensation nuclei modifying the cloud structure (e.g., Forster et al., 2007). Aerosols can either be produced by ejection into the atmosphere or by physical and chemical processes within the atmosphere. Aerosol particles affect the radiative field by attenuating the direct component thereby enhancing (or reducing under a highly absorbing aerosol) the diffuse one. They also produce indirect effects (AIE) by perturbing the Earth's atmospheric radiative balance by modulating cloud albedo and fraction. The AIE can be viewed as a series of processes linking various variables such as aerosol mass, cloud condensation nuclei concentration, ice nuclei concentration, water phase partitioning, cloud optical properties, etc. (Penner et al., 2001).

The aerosol radiative effect (ARE) is defined as the change in net radiation due to changes in atmospheric aerosol properties and content. This is a key quantity in the determination of climate change (e.g., Hansen et al., 1998). Most studies dealing with ARE have focused on discrete wavelengths, whole shortwave (SW) solar radiation spectrum (e.g., Rajeev and Ramanathan, 2001; García et al., 2008; di Sarra et al., 2008; Cachorro et al., 2008; Foyo et al., 2014), longwave (LW) radiation (e.g., Panicker et al., 2008; di Sarra et al., 2011), ultraviolet (UV) interval (e.g., Hatzianastassiou et al., 2004; Kazadzis et al., 2009; Nikitidou et al., 2013), and visible (VIS) range (e.g., Jayaraman et al., 1998; Horvath et al., 2002; Bush and Valero, 2003; Meloni et al., 2003). With regards to surface SW radiative effect (ARE_{SW}), di Sarra et al. (2011) found an ARE_{SW} of $-209\,W\,m^{-2}$ for a strong desert dust intrusion in the Central Mediterranean, and Costa et al. (2006) obtained an ARE_{SW} of $-164.5\ Wm^{-2}$ during an exceptionally absorbing Yellow Sand event off the western coast of Korea. All these negative figures point out a cooling of the Earth's surface. Aerosol radiative effects in the LW (ARE_{LW}) are expected to be smaller than in the SW as di Sarra et al. (2011) obtained a value of +41.5 $W m^{-2}$ for the aforementioned dust event. This heating effect at the surface can partly offset the cooling induced in the SW range. With respect to the ARE for the UV range (ARE_{UV}), Nikitidou et al. (2013) analyzed the ARE in two different spectral regions in the UV range, 300–315 and 315–360 nm. They found a stronger attenuation in the UV-B than in the UV-A, however being both solar zenith angle (SZA) dependent because of different photon paths.

The main goal of this study is to evaluate the ARE at the surface over the Iberian Peninsula, which is a region of great interest because of its geographical position in Southwestern Europe, near the African continent and the interface between the Atlantic Ocean and the Mediterranean Basin. Thus, it is affected by frequent desert dust intrusions which modulate their aerosol climatology (Toledano et al., 2007a; Bennouna et al., 2013; Pey et al., 2013; Valenzuela et al., 2012). In addition, this area is also affected by a great variety of air masses loaded with different aerosol types: clean continental, polluted plumes of central Europe, and marine aerosols. Hence, aerosol climatology at the six stations is also carried out for the time period analyzed in this study. Aerosol radiative effects as well as their efficiency are calculated in four regions of the solar spectrum (ultraviolet, visible, near-infrared, and shortwave) and the relative contribution of each range with respect to the whole solar spectrum is analyzed as a function of the aerosol properties. Therefore, this study is intended to contribute to the understanding of the aerosol impact on radiative budget over the Iberian Peninsula.

This article presents the following outline: detailed descriptions of the aerosol stations and the database used are performed in Sect. 2; Sect. 3 includes the followed methodology; the results obtained in the different analyses about the climatology of aerosol properties, aerosol radiative effects, and aerosol forcing efficiencies are shown and discussed in Sects. 4, 5, and 6, respectively. Finally, the main conclusions of this article are summarized in Sect. 7.

ACPD
14, 8779–8818, 2014

2 Aerosol ground-based data

The aerosol data are obtained from the Aerosol Robotic Network (AERONET) (Holben et al., 1998). Six AERONET sites operating in the Iberian Peninsula are selected in this study: Palencia, Barcelona, Évora, Cabo da Roca, Granada and El Arenosillo (see Table 1), all of them with a minimum of 8 years of data sets of continuous observations.

The standard instrument used in AERONET is the Cimel 318 radiometer. It performs direct sun measurements at selected wavelengths in the spectral range 340–1020 nm. Furthermore, the instrument also measures sky radiance in the solar almucantar and principal plane configurations at 440, 670, 870 and 1020 nm wavelengths. A detailed description of this instrument was provided by Holben et al. (1998). The direct sun observations are used to derive the spectral aerosol optical depth (AOD) and the corresponding Ångström exponent. The sky radiances together with the AOD are employed to retrieve a set of aerosol optical and microphysical properties via inversion methods (Dubovik and King, 2000; Dubovik et al., 2006). These include particle size distribution, complex refractive index, single scattering albedo (SSA), phase function, asymmetry parameter, fraction of non-spherical particles, etc. (see http://aeronet.gsfc.nasa.gov/new_web/Documents/Inversion_products_V2.pdf). Data are provided in three database levels: 1.0 (raw data), 1.5 (cloud-screened) and 2.0 (cloud-screened and quality assured).

The calibration of these instruments is performed following AERONET protocols by AERONET-NASA, PHOTONS and RIMA networks every 12 months of operation approximately. The estimated uncertainty is 0.01–0.02 for AOD (larger at shorter wavelengths) and $\sim 5\,\%$ for the sky radiances (Holben et al., 1998). The SSA has an absolute uncertainty about 0.03–0.05 depending on the aerosol load and type (Dubovik et al., 2000).

Level 2.0 aerosol optical depth data have been used in this work. However, it is well-known that when level 2.0 inversion data are used, the number of available observations of single scattering albedo (SSA) and asymmetry factor (g) is quite limited

ACPD
14, 8779–8818, 2014

because these variables are only considered reliable when $AOD_{440\,nm} > 0.4$[1]. Such AOD is mainly reached in the study region during Saharan dust or biomass burning events, therefore we would not have information on SSA and *g* for other conditions. To solve this issue, we have reduced the threshold of the level 2.0 inversion products. For this, we started with the level 1.5 data (for those quality-assured almucantar data that reached level 2.0) and applied the same criteria used by AERONET to elaborate the level 2.0 regarding the number of symmetrical angles, retrieval error and solar zenith angle (see http://aeronet.gsfc.nasa.gov/new_web/Documents/AERONETcriteria_final1_excerpt.pdf). However, a less restrictive threshold is applied to the AOD, which we restricted to cases with $AOD_{440\,nm} > 0.15$, instead of 0.4. The level 1.5-filtered data of SSA and *g* are daily averaged in order to have one value per day. This approach is a compromise between the amount and the quality of the data and has been adopted by other authors using AERONET absorption data (e.g. Mallet et al., 2013). In these conditions, the estimated uncertainty of the single scattering albedo is ±0.05–0.07 (Dubovik et al., 2000). Furthermore, for those days presenting level 2.0 data but also measurements in the 1.5-filtered level, we tested the uncertainty of our approach. We evaluated the difference in the SSA values of the level 1.5-filtered data with respect to the closest level 2.0 data. The mean relative differences in the SSA values between both methodologies are smaller than 1 %.

Lastly, when the AOD is low (< 0.15 at 400 nm), there is no reliable information on the absorption properties in the almucantar retrievals. Such low AOD is typical in our study region (e.g. almost 70 % of observations at Palencia, Granada and Évora are below this threshold). If only cases with $AOD_{440\,nm} > 0.15$ are considered in our study, the derived aerosol radiative effect would be unrealistically large. To overcome this problem of representativeness, fixed values of SSA (0.90) and *g* (0.75) have been used for the cases with AOD < 0.15 at 440 nm. In spite of the associated uncertainties, we think that our approximation (daily level 1.5-filtered values of these aerosol properties

[1]Other inversion products, like the volume size distributions, are provided for all AOD levels.

ACPD
14, 8779–8818, 2014

for AOD > 0.15 together with a typical fixed value for low AOD cases) provides a good characterization of the aerosol absorption of the particles present in the atmosphere during the investigated period. The data products and AERONET database level are summarized in Table 2, where the estimated absolute uncertainties of AOD and SSA are also provided.

3 Methodology

The ARE calculations are performed in the ultraviolet (ARE_{UV}, 280–400 nm), visible (ARE_{VIS}, 400–700 nm), near-infrared (ARE_{NIR}, 700–2800 nm), and shortwave (ARE_{SW}, 280–2800 nm) intervals. For this purpose, measurements of aerosol properties derived from six sun-photometer datasets under cloud-free conditions are used as input for a radiative transfer code.

The libRadtran model (Mayer and Kylling, 2005) has been shown to be a useful tool for obtaining solar radiation data (e.g., Bilbao et al., 2011; Mateos et al., 2013b). Version 1.7 of the libRadtran is used in this study with inputs of aerosol, total ozone column (TOC), precipitable water vapor column (PWC), and surface albedo data. We performed simulations of ultraviolet (280–400 nm), visible (400–700 nm), near-infrared (700–2800 nm), and shortwave (280–2800 nm) radiation during the periods indicated in Table 1. Total ozone column is provided by the Ozone Monitoring Instrument (OMI) and Total Ozone Mapping Spectrometer (TOMS). Daily values of these instruments are obtained from the Daily Level 3 Global Gridded products, which are downloaded using the Giovanni application (http://disc.sci.gsfc.nasa.gov/giovanni). Level 2.0 AERONET PWC data are used in the calculations. The uncertainty of this parameter is 10–15 % (Holben et al., 1998). In addition, retrievals of surface albedo at 440, 675, 870 and 1020 nm from the AERONET algorithm are also used in this work. For land surface cover, this algorithm relies on the Lie–Ross model (Lucht and Roujean, 2000), but considering the bidirectional reflectance distributions from MODIS (Moody et al., 2005).

ACPD
14, 8779–8818, 2014

Aerosol properties obtained from AERONET measurements are also used as input to the libRadtran model. Ångström coefficients, α and β, are utilized to compute a spectral aerosol optical depth in the wavelengths of interest (Schuster et al., 2006). Ångström exponent α is obtained with the measurements between 440 and 870 nm, while the turbidity β is obtained from the α value and aerosol data at 1020 nm. Since the aerosol asymmetry factor, single scattering albedo, and surface albedo are obtained at four wavelengths from AERONET in each measurement, three different spectral regions are simulated with the libRadtran model. For computations in the UV range (280–400 nm), the AERONET retrievals of aerosol asymmetry factor, aerosol single scattering albedo, and surface albedo at 440 nm are used. The AERONET retrievals at 675 nm of the same variables are used in the visible range (400–700 nm), while in the near-infrared region (700–2800 nm) we used the average properties retrieved at 870 and 1020 nm. In each interval, these properties are considered as wavelength independent. Other options in the model set-up are: extraterrestrial irradiance values are taken from Gueymard (2004); profiles of temperature, air density, ozone and other atmospheric gases are taken from the midlatitude summer/winter standard atmospheres; and the radiative equation solver is the improved version of the discrete ordinate method of Stamnes et al. (2000) (DISORT2) calculated by 16-streams (e.g., de Miguel et al., 2011). After computing the solar irradiance in the different spectral intervals, the SW irradiance is evaluated by adding up the contributions of these three spectral regions.

In order to evaluate the aerosol radiative effect, the simulations under aerosol-free conditions are also computed with the same inputs as explained above, but with a fixed β value of 0.001.

The use of radiative transfer models fed with reliable experimental aerosol data to determine the ARE has been also employed in other studies (e.g., Barja and Antuña, 2011; Valenzuela et al., 2012; García et al., 2014).

ACPD
14, 8779–8818, 2014

Once the simulated radiometric values are obtained, ARE is derived for each interval (X represents UV, VIS, NIR, and SW) at the surface by:

$$\mathrm{ARE}_X = \left(X^{\downarrow}_{\mathrm{aer}} - X^{\uparrow}_{\mathrm{aer}}\right) - \left(X^{\downarrow}_{\mathrm{NOaer}} - X^{\uparrow}_{\mathrm{NOaer}}\right) \tag{1}$$

where X_{aer} and X_{NOaer} are the irradiances ($\mathrm{W\,m^{-2}}$) for the X range under actual and aerosol-free conditions, respectively.

Daily values are obtained by the integration of the hourly data during the whole day (24 h) considering ARE = 0 $\mathrm{W\,m^{-2}}$ for SZA > 90° (e.g., Bush and Valero, 2003; Valenzuela et al., 2012) and assuming cloud-free conditions along the day:

$$\mathrm{ARE}_{\mathrm{daily}} = \sum \mathrm{ARE}_{\mathrm{hourly}} \frac{\mathrm{d}t}{24} \tag{2}$$

The linear relationship between daily aerosol radiative effect and aerosol optical thickness is well known (see, e.g., Costa et al., 2004, 2006; Di Biagio et al., 2009). The aerosol forcing efficiency (AFE) is defined as the radiative effect produced by a unit aerosol optical depth (e.g., Di Biagio et al., 2009; and the references therein). Hence, AFE can be obtained by the slope of linear fits. Linear square methods are applied to daily ARE vs. $\mathrm{AOD}_{500\,\mathrm{nm}}$ relationships to evaluate AFE. AFE values obtained in this study are thus expressed in $\mathrm{W\,m^{-2}}$ per $\mathrm{AOD}_{500\,\mathrm{nm}}$-unit ($\mathrm{W\,m^{-2}}\,\tau^{-1}$).

With respect to the temporal trends calculated in this study, the Mann–Kendall non parametric test is applied with a significant interval of 95 %. This is a common method in temporal trend evaluation (e.g., Mateos et al., 2013a).

4 Climatological analysis of aerosol properties over the Iberian Peninsula

A direct CIMEL retrieval (AOD at 440 nm) is selected to perform the climatological analysis because the estimations of $\mathrm{AOD}_{500\,\mathrm{nm}}$ (used in the ARE calculations) are obtained using α values. Hence, we minimized the impact of other uncertainty sources in the

ACPD
14, 8779–8818, 2014

AOD analysis. Besides, the results for $AOD_{440\,nm}$ and $AOD_{500\,nm}$ do not differ excessively. In order to identify the differences in the aerosol climatology over the six sites analyzed in this study, the monthly distribution of the daily values of the $AOD_{440\,nm}$ and α are evaluated using the database mentioned in Table 1. All the available level 2.0 AERONET measurements are used in this section.

Figure 1 shows the climatology of the aerosol load by box whisker plots. Several conclusions can be drawn from this figure. The highest values of the AOD occur in Barcelona, as can be expected because it is a large city. With respect to the monthly average values (triangles in the figure), the central stations in the Iberian Peninsula (Palencia and Évora) exhibit $AOD_{440\,nm}$ below 0.2, while the southern sites (Cabo da Roca, Granada, and El Arenosillo) show aerosol load over 0.2 during summer months. The $AOD_{440\,nm}$ seasonal distribution is seen, with maximum values in summer and minimum ones in winter. However, the seasonality becomes more evident in the stations outside the central area of the Iberian Peninsula. The large differences between median and average values for some months evidence a large impact of high aerosol optical depth events on the monthly climatology. In this line, the bimodality of the monthly AOD climatology (with two maximum monthly means occurring in March and summer months) observed for the El Arenosillo site has been already reported by previous studies (e.g., Bennouna et al., 2011), and directly attributed to desert dust intrusions from the African continent.

To go further in the characterization, α allows for a better understanding of the particle size over each site. Figure 2 shows the climatology of this variable over the six stations using also box whisker plots. Analyzing the monthly average means, α values larger than one, indicative of the predominance of fine particles, are dominant over Barcelona, Palencia, and Évora. The other three stations (Cabo da Roca, Granada, and El Arenosillo) present monthly α averages over and below 1, which means a larger variety of aerosol sizes over these stations. A seasonal dependence over Granada site is seen, with winter months dominated by fine particles (see also Lyamani et al., 2012) and summer months by larger ones (see also Navas-Guzman et al., 2013). Values

ACPD
14, 8779–8818, 2014

of α present a large variability during summer, indicative of the influence of different aerosol types including biomass burning events and Saharan dust transport (e.g., Pérez-Ramirez, 2008). The monthly distribution of α is symmetric with similar average and median values through the year for the six sites.

With the daily AOD and α values, it is possible to classify the origin of the aerosol particles. Previous studies suggest different thresholds of AOD and α (e.g., Hess et al., 1998; Pace et al., 2006; Toledano et al., 2007b), i.e., these limits are site-dependent. A simple classification, which can be used for the whole Iberian Peninsula, of aerosol type is carried out in this study. The threshold between fine and large particles is placed at $\alpha = 1$, while the situations with a high aerosol load are those with $AOD_{440\,nm} > 0.2$. Therefore, aerosol particles can be classified in four types: maritime ($AOD_{440\,nm} < 0.2$ and $\alpha < 1$), desert dust ($AOD_{440\,nm} > 0.2$ and $\alpha < 1$), continental clean ($AOD_{440\,nm} < 0.2$ and $\alpha > 1$), and continental polluted ($AOD_{440\,nm} > 0.2$ and $\alpha > 1$). Note that the limit of $AOD_{440\,nm} < 0.2$ is arbitrary and this value could be adjusted according to the sites, which likely produce a different distribution different distribution in the pie diagrams. However it is not the aim of this work to provide an extensive aerosol climatology, but rather to demonstrate the great variety of air masses over Iberia which transport different aerosol types. Although other types, such as biomass burning or mixed aerosols, are placed in the boundaries of these types, this simple classification can provide information about the aerosol sources for the six sites. Figure 3 shows pie diagrams with the frequency of occurrence of the four aerosol types. The six diagrams agree pointing at continental clean as the main type of aerosols over the Iberian Peninsula. In Barcelona, there is also an important contribution of continental polluted, since Barcelona is a large coastal city with relevant pollution levels from vehicular and ship traffic (e.g., Reche et al., 2011). The influence of maritime aerosols is notable at El Arenosillo, Cabo da Roca, and Évora sites (Toledano et al., 2007a; Bennouna et al., 2011; Obregón et al., 2012). Furthermore, desert dust events are shown to be common in the Iberian Peninsula with a higher occurrence at Granada and El Arenosillo sites (the two closest points to the African continent and hence to the Saharan desert) (see also Toledano et al., 2007b; Guerrero-Rascado et al., 2008; Antón et al., 2012b). For instance, the minimum values of α obtained for Granada station during summer months are linked to the higher likelihood of desert dust events (Valenzuela et al., 2012), being sometimes associated with high aerosol loads (Córdoba-Jabonero et al., 2011). These results corroborate the findings obtained by previous studies about desert dust events over the Iberian Peninsula (see, e.g., Lyamani et al., 2005; Cachorro et al., 2006, 2008; Toledano et al., 2007b).

The temporal trend of aerosol load can be established over the last decade in the Iberian Peninsula. The yearly values of $AOD_{440\,nm}$ at the six sites are shown in Fig. 4. Overall, the evolution of these yearly values is weak. The evaluation of the temporal trends (Mann–Kendall test with the 95 % significance level) only produces one statistically significant trend for the Barcelona site, where a decrease of the aerosol load of 0.09 $AOD_{440\,nm}$-unit per decade is observed. Although the results obtained for the other sites are not statistically significant, the sign of the temporal trends is negative for all of them. In particular, Évora and Palencia stations showed trend rates of −0.06 and −0.04 $AOD_{440\,nm}$-unit per decade with significance levels of 94 % and 90 %, respectively. Hence, a slight reduction of the aerosol load over the Iberian Peninsula is observed since 2000. This result obtained in the Southeastern Europe is in line with the long-term analysis of AOD series performed in Northern Germany and Switzerland by Ruckstuhl et al. (2008). These authors highlight a strong decrease of aerosol load starting in 1985, while the values are stabilized since about 2000.

5 Inter-annual and intra-annual evolution of ARE

From the daily ARE values, the yearly ARE averages for each station and spectral range are evaluated to analyze their inter-annual changes (see Fig. 5). In spite of the high variability of the yearly values with large standard deviations (see the vertical bars for Palencia station in the figure), the radiative effects of atmospheric aerosols have slightly declined over the last years. The ARE_{UV} and ARE_{VIS} are

ACPD
14, 8779–8818, 2014

the primary components that show substantial inter-annual changes, while ARE_{NIR} presents a more stable pattern. The significance level of the temporal trends (Mann–Kendall nonparametric test at the 95 % confidence interval) are evaluated, and Évora and Palencia sites exhibit statistically significant trends during this period. The trends for the aerosol effects for Palencia (Évora) are: +4.9 (+3.2) $W m^{-2}$ per decade in ARE_{SW}, +3.3 (+2.1) $W m^{-2}$ per decade in ARE_{VIS}, +0.1 (+0.08) $W m^{-2}$ per decade in ARE_{NIR}, and +0.06 (+0.03) $W m^{-2}$ per decade in ARE_{UV}. The other four stations present positive trends in all the spectral ranges, but they are not statistically significant at the 95 % confidence interval. This slight reduction in the radiative effects of the atmospheric aerosol over the Iberian Peninsula could partially contribute to the increase in the levels of SW radiation at the surface (the brightening phenomenon) in this region reported by Sanchez-Lorenzo et al. (2013) and Mateos et al. (2013a).

To establish the general behavior of the ARE over the whole Iberian Peninsula, the annual averages using the six ground-based stations are evaluated. Only those years with, at least, simultaneous measurements at three sites are considered in these averages, and consequently, the time period is limited to 2004–2012. Figure 6 shows the evolution of the ARE and AOD at 500 nm for the entire peninsula. A reduction of the aerosol load over the peninsula is observed during this period, with the consequent decrease in the aerosol radiative effect at the four spectral ranges. The temporal trends of these annual values are evaluated, and all the trends resulted statistically significant at the 95 % significance level are shown in Fig. 6. Overall, ARE_{SW} over the Iberian Peninsula increased 3.6 $W m^{-2}$ per decade while the aerosol reduced 0.04 $AOD_{500\,nm}$-unit per decade. The annual means of aerosol radiative effects over the entire peninsula are in the ranges: $-1.1 < ARE_{UV} < -0.7\,W m^{-2}$, $-5.7 < ARE_{VIS} < -3.8\,W m^{-2}$, $-2.8 < ARE_{NIR} < -1.7\,W m^{-2}$, and $-9.5 < ARE_{SW} < -6.1\,W m^{-2}$. The larger contribution of the visible spectral region with respect to the whole solar spectrum was also noticed by Bush and Valero (2003). The relationship between ARE and $AOD_{500\,nm}$ is analyzed more in detail in Sect. 6, when the aerosol forcing efficiency is evaluated for each ground-based station.

ACPD
14, 8779–8818, 2014

In addition to the inter-annual changes, the intra-annual behavior is also analyzed. For this purpose, the annual cycle (12 monthly averages) is evaluated for the six stations (see Fig. 7). A seasonal pattern is seen in ARE_{UV} and ARE_{VIS}, and therefore, ARE_{SW}. However, ARE_{NIR} does not follow a seasonal pattern, particularly at the Évora and Palencia stations given that ARE_{NIR} remains nearly constant. Small differences among the six stations are observed in the annual cycle during the cold seasons. The aerosol radiative effects are stronger during summer months. This can be related to the higher likelihood of desert dust or biomass burning events over the Iberian Peninsula in these months (e.g., Cachorro et al., 2008; Valenzuela et al., 2012), as was mentioned above. This is corroborated by the increase of the differences among the stations during the warm season, likely due to the variability in the impact of the desert dust episodes which strongly depend on the geographical location of each site. The higher occurrence of large aerosol loads during the warm seasons (see Fig. 1), can explain the more negative ARE during summer and spring in Fig. 7. For instance, the Barcelona station, with the largest values of $AOD_{440\,nm}$, is the bottom curve of each panel in Fig. 7. Furthermore, the influence of mineral dust aerosol (with high aerosol optical depth) during these months also causes strong radiative effects, as was also reported by previous studies (e.g., Cachorro et al., 2008; Guerrero-Rascado et al., 2009; Antón et al., 2012a, b; Román et al., 2013; García et al., 2014). In addition, the bimodality of the monthly AOD climatology mentioned in Sect. 4 has its impact on the radiative effects. The annual AOD cycle (see Fig. 1, El Arenosillo site) causes the inverse monthly distribution of ARE with a first minimum in March. This effect is more clearly seen in ARE_{NIR} and ARE_{SW}.

6 Aerosol radiative forcing efficiency in different spectral ranges

The daily AFE values are calculated (following the methodology described in Sect. 3) in all the spectral ranges. AFE is a function of the aerosol optical properties, where both the aerosol particle size distribution and absorptive properties play a key role (e.g., Antón et al., 2011). As we assumed a fixed value of SSA = 0.90 in the simulations with $AOD_{440\,nm} < 0.15$ (see Table 2), the AFE is calculated only for those cases showing $AOD_{440\,nm}$ larger than 0.15.

To identify the influence of SSA and α on AFE, this variable is calculated for several intervals of each aerosol property. Four categories of single scattering albedo at 675 nm are established in the calculation of the AFE: $1.0 \geq SSA_1 > 0.95$, $0.95 \geq SSA_2 > 0.90$, $0.90 \geq SSA_3 > 0.85$, and $0.85 \geq SSA_4 > 0.80$. Furthermore, aerosol size is classified in three intervals: $0 \leq \alpha_1 \leq 1$, $1 < \alpha_2 \leq 1.5$, and $1.5 < \alpha_3 \leq 2$. Note that two intervals in the range of α larger than 1 have been considered. One for median particles and another one for fine particles, because of the relevant importance of median size particle (continental or mixed aerosol aerosols types) over the Iberian Peninsula (see Fig. 3). Although the general classification between fine and coarse particles requires a more refined classification (Schuster et al., 2006; Prats et al., 2011), the more general intervals selected in this study are adequate to perform a study of the aerosol sizes at the six stations together.

Figure 8 shows the AFE obtained for the UV (AFE_{UV}), VIS (AFE_{VIS}), NIR (AFE_{NIR}), and SW (AFE_{SW}) ranges for all these intervals. The threshold to evaluate the average in each sub-interval is fixed at 10 data points. From these figures it is seen that, the stronger the absorption by aerosols, the stronger their forcing efficiency. That is a decrease in the absolute values of the AFE is observed for increasing SSA for all particle size. In general, the groups of non-absorbing particles exhibit a good agreement among the six stations (see, for instance, AFE values in all the spectral ranges in the interval $1 < \alpha \leq 1.5$). Larger differences are obtained in the case of more absorbing aerosol particles. These can be understood because of the different types of aerosols presented over each site (see Sect. 4) and the different data numbers. The average AFE values over the whole Iberian Peninsula (considering the six stations together) are presented in Table 3 as a function of α and SSA, separately. The role played by the aerosol size on AFE values is different in the three sub-intervals of the shortwave radiation. AFE_{UV} and AFE_{VIS} are larger (in absolute value) for fine particles, while the opposite occurs in the case of AFE_{NIR}. As a result of these mixed effects, AFE_{SW} shows also a decrease in its values with increasing α, but this effect is weaker than for the visible and ultraviolet part. SSA exhibits a more dominant role. As was observed before, the most negative values are achieved for the most absorbing aerosols considered in this study (group 1 of SSA, see Table 3). AFE_{NIR} shows the weakest effect caused by aerosol absorption.

The average values of forcing efficiency obtained in this study (see Table 3) are in line with those found by other authors. Díaz et al. (2007) obtained values between −2.72 and −3.22 $W\,m^{-2}\,\tau^{-1}$ in the spectral interval 290–363 nm. Regarding AFE_{VIS}, Meloni et al. (2005) obtained values between −28.4 (desert dust) and 45.6 (mixed types) $W\,m^{-2}\,\tau^{-1}$, while Lyamani et al. (2006) computed values of −78.2 and −73.4 $W\,m^{-2}\,\tau^{-1}$ in Granada during the 2003 heat wave that affected large parts of Europe. AFE_{SW} obtained by other authors are: −116.9 $W\,m^{-2}\,\tau^{-1}$ for a single scattering albedo of 0.76 (Costa et al., 2006); −113.0 and −66.0 $W\,m^{-2}\,\tau^{-1}$ (Santos et al., 2008); −120.5 and −59.0 $W\,m^{-2}\,\tau^{-1}$ (Di Biagio et al., 2010); −74 and −65 $W\,m^{-2}\,\tau^{-1}$ (Valenzuela et al., 2012); −97.6 and −68.1 $W\,m^{-2}\,\tau^{-1}$ (Saha et al., 2008); −90 and −50 $W\,m^{-2}\,\tau^{-1}$ (Zhou et al., 2005); −139 $W\,m^{-2}\,\tau^{-1}$ (Esteve et al., 2014); and −59 $W\,m^{-2}\,\tau^{-1}$ (García et al., 2014). As was noticed by, e.g., Costa et al. (2004, 2006) and Di Biagio et al. (2010), AFE at the surface is larger (in absolute term) for aerosols characterized by smaller and absorbing particles. This result is corroborated by the findings shown in this study. Furthermore, as was pointed out by Di Biagio et al. (2010), the aerosol absorption is the dominant factor on AFE evaluated at the surface.

To evaluate the contribution of each spectral range with respect to the shortwave, the dependence of each AFE ratio (VIS to SW and NIR to SW) on SSA and α is shown in Fig. 9. AFE_{VIS}/AFE_{SW} and AFE_{NIR}/AFE_{SW} ratios are shown in the figure since their contributions are the dominant. AFE_{UV}/AFE_{SW} ratio can be obtained as 100 % minus the sum of the percentage of the two other ranges. As expected, non substantial differences are observed in the behavior of the six stations considered in this study. The NIR contribution becomes more decisive for large particles ($\alpha < 1$). It is expected that larger particles interact more with the longer wavelengths, while the smaller particles

Discussion Paper | Discussion Paper | Discussion Paper | Discussion Paper |
ACPD
14, 8779–8818, 2014

present more interaction with the shorter wavelengths. The presence of large particles with low SSA (high absorption) leads to a reduction of the AFE_{NIR}/AFE_{SW} ratio as well as an increase of the AFE_{VIS}/AFE_{SW} ratio. However, for non-absorbing (high SSA) large particles, the AFE_{NIR}/AFE_{SW} ratio increases, and the contributions of the visible and infrared parts become more similar (both around ~ 40–50 %). The difference between AFE_{VIS}/AFE_{SW} and AFE_{NIR}/AFE_{SW} increases for intermediate – fine particles. For these particles, the AFE_{VIS}/AFE_{SW} ratio does not show a dependence on SSA. The smallest contribution of the NIR interval is around ~ 25 % under strong absorbing aerosols and fine particles, while AFE_{VIS}/AFE_{SW} is still over 60 %. For this case, the contribution of the ultraviolet range achieves a maximum of ~ 15 %, being almost comparable with the near infrared contribution. In summary, aerosol size determines the relevance of VIS-NIR ranges, while SSA plays a key role, particularly, for large particles.

7 Conclusions

Six long-term datasets of aerosol properties over the Iberian Peninsula were analyzed and used as input in a radiative transfer model to simulate ultraviolet, visible, near-infrared, and shortwave radiation. The aerosol radiative effect (ARE) and aerosol forcing efficiency (AFE) were calculated. The main conclusions are as follows:

1. The annual cycles of AOD and α values of atmospheric aerosols over the six analyzed stations present high variability among them, emphasizing the inhomogeneity of the Iberian Peninsula, mainly due to the different aerosol types over each station. The Barcelona site presents the largest values of AOD, although Southern stations (Granada and El Arenosillo sites) frequently exhibit daily values over 0.2 during summer months. The classification α-AOD has shown that continental (mainly, clean) is the principal type of aerosol over the Iberian Peninsula. However, maritime aerosols are also common in the Cabo da Roca, El Arenosillo

ACPD
14, 8779–8818, 2014

and Évora sites. Desert dust events are registered at the six sites, with the highest frequency at Granada and El Arenosillo, but the most relevant feature is the South–North gradient of desert dust load which modulates the aerosol climatology over the Iberian Peninsula.

2. The aerosol load over the Iberian Peninsula has shown a decrease trend between 2004 and 2012 (−0.04 per unit of $AOD_{500\,nm}$ per decade, being statistically significant at the 95 % of significance level). Yearly values of the AOD at 440 nm have also shown a statistically significant trend of −0.09 $AOD_{440\,nm}$-unit per decade at Barcelona site. The temporal trends for the rest of the stations are not statistically significant at the 95 % significance level, but all of them are negative. Hence, a reduction of the aerosol column load over the Iberian Peninsula is observed in the last decade.

3. In the whole Iberian Peninsula, yearly ARE_{UV} ranges between −1.1 and −0.7 $W\,m^{-2}$, ARE_{VIS} ranges between −5.7 and −3.8 $W\,m^{-2}$, and ARE_{NIR} has values between −9.5 and −6.1 $W\,m^{-2}$. As a result, ARE_{SW} is in the range between −9.5 and −6.1 $W\,m^{-2}$. The temporal trends of ARE_{UV}, ARE_{VIS}, ARE_{NIR}, and ARE_{SW} exhibit positive statistically significant trends between 2004 and 2012. For instance, the trend rate for the ARE_{SW} is +3.6 $W\,m^{-2}$ per decade (statistically significant at the 95 % of significance level).

4. The intra-annual ARE cycle exhibits larger values during the spring and summer months when the likelihood of high aerosol loading over the Iberian Peninsula increases. In general, the annual AOD cycle is driven by the occurrence of Saharan dust events.

5. The AFE values at the six stations used in this study are in good agreement. Conditions of high α (small particles predominate) and low SSA (high absorption) lead to the largest negative AFE values. Overall, as an average for

ACPD
14, 8779–8818, 2014

the Iberian Peninsula: $AFE_{UV} = -6\,W\,m^{-2}\,\tau^{-1}$, $AFE_{VIS} = -34\,W\,m^{-2}\,\tau^{-1}$, $AFE_{NIR} = -19\,W\,m^{-2}\,\tau^{-1}$, and $AFE_{SW} = -59\,W\,m^{-2}\,\tau^{-1}$.

6. The contribution of the ultraviolet, visible, and infrared to total shortwave aerosol forcing efficiency is governed by the aerosol type. In general, the visible part of the spectrum is the most dominant part. Non-absorbing large particles cause a more equal contribution of VIS and NIR intervals, while the UV range shows a higher contribution for absorbing fine particles.

Acknowledgements. The work is supported by the Spanish Ministry of Science and Technology (currently MINECO) through projects CGL2010-18782, CSD2007-00067, CGL2011-29921-C02-01, CGL2011-23413, CGL2011-24891, CGL2011-13085-E, CGL2011-13580-E, CGL2012-33576, and CGL2012-33576; FEDER (Programa Operacional Factores de Competitividade – COMPETE). Also by Portuguese funding through FCT – Fundação para a Ciência e a Tecnologia in the framework of project FCOMP-01-0124-FEDER-009303 (PTDC/CTE-ATM/102142/2008); the Évora Geophysics Centre, Portugal, under the contract with FCT, PEst-OE/CTE/UI0078/2014; and the Andalusia Regional Government through projects P08-RNM-3568 and P10-RNM-6299. The research leading to these results has received also funding from the European Union Seventh Framework Programme (FP7/2007-2013) under grant agreement no. 262254 [ACTRIS]. Manuel Antón and Carlos Toledano thank Ministerio de Ciencia e Innovación and Fondo Social Europeo for the awards of a postdoctoral grant (Ramón y Cajal), and Mar Sorribas for postdoctoral grant (Juan de la Cierva). We must specially thank the AERONET-GSFC, PHOTONS-LOA and RIMA-GOA-UVa staff for their scientific and technical support. Ozone Monitoring Instrument (OMI) and Total Ozone Mapping Spectrometer (TOMS) ozone column data were obtained from the Giovanni online data system, developed and maintained by the NASA GES DISC.

References

Antón, M., Gil, J. E., Fernández-Gálvez, J., Lyamani, H., Valenzuela, A., Foyo-Moreno, I., Olmo, F. J., and Alados-Arboledas, L.: Evaluation of the aerosol forcing efficiency

in the UV erythemal range at Granada, Spain, J. Geophys. Res., 116, D20214, doi:10.1029/2011JD016112, 2011.
Antón, M., Sorribas, M., Bennouna, Y., Vilaplana, J. M., Cachorro, V. E., Gröbner, J., and Alados-Arboledas, L.: Effects of an extreme desert dust event on the spectral ultraviolet irradiance at El Arenosillo (Spain), J. Geophys. Res., 117, D03205, doi:10.1029/2011JD016645, 2012a.
Antón, M., Valenzuela, A., Cazorla, A., Gil, J. E., Fernández-Gálvez, J., Lyamani, H., Foyo-Moreno, I., Olmo, F. J., and Alados-Arboledas, L.: Global and diffuse shortwave irradiance during a strong desert dust episode at Granada (Spain), Atmos. Res., 118, 232–239, doi:10.1016/j.atmosres.2012.07.007, 2012b.
Barja, B. and Antuña, J. C.: The effect of optically thin cirrus clouds on solar radiation in Camagüey, Cuba, Atmos. Chem. Phys., 11, 8625–8634, doi:10.5194/acp-11-8625-2011, 2011.
Bennouna, Y., Cachorro, V., Toledano, C., Berjón, A., Prats, N., Fuertes, D., Gonzalez, R., Rodrigo, R., Torres, B., and de Frutos, A.: Comparison of atmospheric aerosol climatologies over southwestern Spain derived from AERONET and MODIS, Remote Sens. Environ., 115, 1272–1284, 2011.
Bennouna, Y. S., Cachorro, V. E., Torres, B., Toledano, C., Berjón, A., de Frutos, A. M., and Fernández-Coopel, A.: Atmospheric turbidity determined by the annual cycle of the aerosol optical depth over north-center Spain from ground (AERONET) and satellite (MODIS), Atmos. Environ., 67, 352–364, doi:10.1016/j.atmosenv.2012.10.065, 2013.
Bilbao, J., Román, R., de Miguel, A., and Mateos, D.: Long-term solar erythemal UV irradiance data reconstruction in Spain using a semiempirical method, J. Geophys. Res., 116, D22211, doi:10.1029/2011JD015836, 2011.
Bush, B. C. and Valero, F. P. J.: Surface aerosol radiative forcing at Gosan during the ACE–Asia campaign, J. Geophys. Res., 108, 8660, doi:10.1029/2002JD003233, 2003.
Cachorro, V. E., Vergaz, R., de Frutos, A. M., Vilaplana, J. M., Henriques, D., Laulainen, N., and Toledano, C.: Study of desert dust events over the southwestern Iberian Peninsula in year 2000: two case studies, Ann. Geophys., 24, 1493–1510, doi:10.5194/angeo-24-1493-2006, 2006.
Cachorro, V. E., Toledano, C., Prats, N., Sorribas, M., Mogo, S., Berjón, A., Torres, B., Rodrigo, R., de la Rosa, J., and De Frutos, A. M.: The strongest desert dust intrusion mixed with smoke over the Iberian Peninsula registered with Sun photometry, J. Geophys. Res., 113, D14S04, doi:10.1029/2007JD009582, 2008.

Córdoba-Jabonero, C., Sorribas, M., Guerrero-Rascado, J. L., Adame, J. A., Hernández, Y., Lyamani, H., Cachorro, V., Gil, M., Alados-Arboledas, L., Cuevas, E., and de la Morena, B.: Synergetic monitoring of Saharan dust plumes and potential impact on surface: a case study of dust transport from Canary Islands to Iberian Peninsula, Atmos. Chem. Phys., 11, 3067–3091, doi:10.5194/acp-11-3067-2011, 2011.

Costa, M. J., Levizzani, V., and Silva, A. M.: Aerosol characterization and direct radiative forcing assessment over the ocean. Part II: Application to test cases and validation, J. Appl. Meteorol., 43, 1818–1833, doi:10.1175/JAM2157.1, 2004.

Costa, M. J., Sohn, B. J., Levizzani, V., and Silva, A. M.: Radiative forcing of Asian dust determined from the synergized GOME and GMS satellite data – a case study, J. Meteorol. Soc. Jpn., 84, 85–95, doi:10.2151/jmsj.84.85, 2006.

de Miguel, A., Mateos, D., Bilbao, J., and Román, R.: Sensitivity analysis of ratio between ultraviolet and total shortwave solar radiation to cloudiness, ozone, aerosols and precipitable water, Atmos. Res., 102, 136–144, doi:10.1016/j.atmosres.2011.06.019, 2011.

Di Biagio, C., di Sarra, A., Meloni, D., Monteleone, F., Piacentino, S., and Sferlazzo, D.: Measurements of mediterranean aerosol radiative forcing and influence of the single scattering albedo, J. Geophys. Res., 114, D06211, doi:10.1029/2008JD011037, 2009.

Di Biagio, C., di Sarra, A., and Meloni, D.: Large atmospheric shortwave radiative forcing by Mediterranean aerosols derived from simultaneous ground-based and spaceborne observations and dependence on the aerosol type and single scattering albedo, J. Geophys. Res., 115, D10209, doi:10.1029/2009JD012697, 2010.

di Sarra, A., Pace, G, Meloni, D., De Silvestri, L., Piacentino, S., and Monteleone, F.: Surface shortwave radiative forcing of different aerosol types in the Mediterranean, Geophys. Res. Lett., 35, L02714, doi:10.1029/2007GL032395, 2008.

di Sarra, A., Di Biagio, C., Meloni, D., Monteleone, F., Pace, G., Pugnaghi, S., and Sferlazzo, D.: Shortwave and longwave radiative effects of the intense Saharan dust event of 25–26 March 2010 at Lampedusa (Mediterranean Sea), J. Geophys. Res., 116, D23209, doi:10.1029/2011JD016238, 2011.

Díaz, A. M., García, O. E., Díaz, J. P., Expósito, F. J., Utrillas, M. P., Martínez-Lozano, J. A., Alados-Arboledas, L., Olmo, F. J., Lorente, J., Cachorro, V., Horvath, H., Labajo, A., Sorribas, M., Vilaplana, J. M., Silva, A. M., Elias, T., Pujadas, M., Rodrigues, J. A., and González, J. A.: Aerosol radiative forcing efficiency in the UV region over southeastern Mediterranean:

VELETA2002 campaign, J. Geophys. Res., 112, D06213, doi:10.1029/2006JD007348, 2007.
Dubovik, O. and King, M. D.: A flexible inversion algorithm for retrieval of aerosol optical properties from Sun and sky radiance measurements, J. Geophys. Res., 105, 20673–20696, 2000.
Dubovik, O., Smirnov, A., Holben, B. N., King, M. D., Kaufman, Y. J., Eck, T. F., and Slutsker, I.: Accuracy assessments of aerosol optical properties retrieved from Aerosol Robotic Network (AERONET) Sun and sky radiance measurements, J. Geophys. Res., 105, 9791–9806, 2000.
Dubovik, O., Sinyuk, A., Lapynok, T., Holben, B. N., Mischenko, M., Yang, P., Eck, T. F., Volten, H., Muñoz, O., Veihelmann, B., van der Zande, W. J., Leon, J. F., Sorokin, M., and Slutsker, I.: Application of spheroid models to account for aerosol particle nonsphericity in remote sensing of desert dust, J. Geophys. Res., 111, D11208, 2006.
Esteve, A. R., Estellés, V., Utrillas, M. P., and Martínez-Lozano, J. A.: Analysis of the aerosol radiative forcing over a Mediterranean urban coastal site, Atmos. Res., 137, 194–204, doi:10.1016/j.atmosres.2013.10.009, 2014.
Forster, P., Ramaswamy, V., Artaxo, P., Berntsen, T., Betts, R., Fahey, D. W., Haywood, J., Lean, J., Lowe, D. C., Myhre, G., Nganga, J., Prinn, R., Raga, G., Schulz, M., and Van Dorland, R.: Changes in atmospheric constituents and in radiative forcing, in: Climate Change 2007: The Physical Science Basis. Contribution of Working Group I to the Fourth Assessment Report of the Intergovernmental Panel on Climate Change, edited by: Solomon, S. et al., Cambridge Univ. Press, Cambridge, UK, 129–234, 2007.
Foyo-Moreno, I., Alados, I., Antón, M., Fernández-Gálvez, J., Cazorla, A., and Alados-Arboledas, L.: Estimating aerosol characteristics from solar irradiance measurements at an urban location in Southeastern Spain, J. Geophys. Res.-Atmos., 119, 1845–1859, doi:10.1002/2013JD020599, 2014.
García, O. E., Díaz, A. M., and Expósito, F. J.: Validation of AERONET estimates of atmospheric solar fluxes and aerosol radiative forcing by ground-based broadband measurements, J. Geophys. Res., 113, D21207, doi:10.1029/2008JD010211, 2008.
García, R. D., García, O. E., Cuevas, E., Cachorro, V. E., Romero-Campos, P. M., Ramos, R., and de Frutos, A. M.: Solar radiation measurements compared to simulations at the BSRN Izaña station: mineral dust radiative forcing and efficiency study, J. Geophys. Res.-Atmos., 119, 179–194, doi:10.1002/2013JD020301, 2014.

ACPD
14, 8779–8818, 2014

ARF Iberian Peninsula

D. Mateos et al.

Guerrero-Rascado, J. L., Ruiza, B., and Alados-Arboledas, L.: Multi-spectral Lidar characterization of the vertical structure of Saharan dust aerosol over southern Spain, Atmos. Environ., 42, 2668–2681, 2008.
Guerrero-Rascado, J. L., Olmo, F. J., Avilés-Rodríguez, I., Navas-Guzmán, F., Pérez-Ramírez, D., Lyamani, H., and Alados Arboledas, L.: Extreme Saharan dust event over the southern Iberian Peninsula in september 2007: active and passive remote sensing from surface and satellite, Atmos. Chem. Phys., 9, 8453–8469, doi:10.5194/acp-9-8453-2009, 2009.
Gueymard, C.: The sun's total and spectral irradiance for solar energy applications and solar radiation models, Sol. Energy, 76, 423–453, 2004.
Hansen, J. E., Sato, M., Lacis, A., Ruedy, R., Tegen, I., and Matthews, E.: Climate forcings in the industrial era, P. Natl. Acad. Sci. USA, 95, 12753–12758, doi:10.1073/pnas.95.22.12753, 1998.
Hatzianastassiou, N., Katsoulis, B., and Vardavas, I.: Global distribution of aerosol direct radiative forcing in the ultraviolet and visible arising under clear skies, Tellus B, 56, 51–71, doi:10.1111/j.1600-0889.2004.00085.x, 2004.
Hess, M., Koepke, P., and Schult, I.: Optical properties of aerosols and clouds: the software package OPAC, B. Am. Meteorol. Soc., 79, 831–844, 1998.
Holben, B. N., Eck, T. F., Slutsker, I., Tanré, D., Buis, J. P., Setzer, A., Vermote, E., Reagan, J. A., Kaufman, Y. J., Nakajima, T., Lavenu, F., Jankowiak, I., and Smirnov, A.: AERONET – a federated instrument network and data archive for aerosol characterization, Remote Sens. Environ., 66, 1–16, 1998.
Horvath, H., Alados Arboledas, L., Olmo, F. J., Jovanovic, O., Gangl, M., Kaller, W., Sánchez, C., Sauerzopf, H., and Seidl, S.: Optical characteristics of the aerosol in Spain and Austria and its effect on radiative forcing, J. Geophys. Res., 107, 4386, doi:10.1029/2001JD001472, 2002.
Jayaraman, A., Lubin, D., Ramachandran, S., Ramanathan, V., Woodbridge, E., Collins, W. D., and Zalpuri, K. S.: Direct observations of aerosol radiative forcing over the tropical Indian Ocean during the Janauary–February 1996 pre-INDOEX cruise, J. Geophys. Res., 103, 13827–13836, doi:10.1029/98JD00559, 1998.
Kazadzis, S., Kouremeti, N., Bais, A., Kazantzidis, A., and Meleti, C.: Aerosol forcing efficiency in the UVA region from spectral solar irradiance measurements at an urban environment, Ann. Geophys., 27, 2515–2522, doi:10.5194/angeo-27-2515-2009, 2009.
Lucht, W. and Roujean, J. L.: Consideration in parametric modelling of BRDF and albedo from multi-angular satellite sensors observations, Remote Sens. Rev., 18, 343–379, 2000.

Lyamani, H., Olmo, F. J., and Alados-Arboledas, L.: Saharan dust outbreak over southeastern Spain as detected by sun photometer, Atmos. Environ., 39, 7276–7284, doi:10.1016/j.atmosenv.2005.09.011, 2005.

Lyamani, H., Olmo, F. J., Alcántara, A., and Alados-Arboledas, L.: Atmospheric aerosols during the 2003 heat wave in southeastern Spain II: microphysical columnar properties and radiative forcing, Atmos. Environ., 40, 6465–6476, doi:10.1016/j.atmosenv.2006.04.047, 2006.

Lyamani, H., Fernández-Gálvez, J., Pérez-Ramírez, D., Valenzuela, A., Antón, M., Alados, I., Titos, G., Olmo, F. J., and Alados-Arboledas, L.: Aerosol properties over two urban sites in South Spain during an extended stagnation episode in winter season, Atmos. Environ., 62, 424–432, 2012.

Mallet, M., Dubovik, O., Nabat, P., Dulac, F., Kahn, R., Sciare, J., Paronis, D., and Léon, J. F.: Absorption properties of Mediterranean aerosols obtained from multi-year ground-based remote sensing observations, Atmos. Chem. Phys., 13, 9195–9210, doi:10.5194/acp-13-9195-2013, 2013.

Mateos, D., Antón, M., Sanchez-Lorenzo, A., Calbó, J., and Wild, M.: Long-term changes in the radiative effects of aerosols and clouds in a mid-latitude region (1985–2010), Global Planet. Change, 111, 288–295, doi:10.1016/j.gloplacha.2013.10.004, 2013a.

Mateos, D., Antón, M., Valenzuela, A., Cazorla, A., Olmo, F. J., and Alados-Arboledas, L.: Shortwave radiative forcing at the surface for cloudy systems at a midlatitude site, Tellus B, 65, 21069, doi:10.3402/tellusb.v65i0.21069, 2013b.

Mayer, B. and Kylling, A.: Technical note: The libRadtran software package for radiative transfer calculations - description and examples of use, Atmos. Chem. Phys., 5, 1855–1877, doi:10.5194/acp-5-1855-2005, 2005.

Meloni, D., di Sarra, A., DeLuisi, J., Di Iorio, T., Fiocco, G., Junkerman, W., and Pace, G.: Tropospheric aerosols in the Mediterranean: 2. radiative effects through model simulations and measurements, J. Geophys. Res., 108, 4317, doi:10.1029/2002JD002807, 2003.

Meloni, D., di Sarra, A., Di Iorio, T., and Fiocco, G.: Influence of the vertical profile of Saharan dust on the visible direct radiative forcing, J. Quant. Spectrosc. Ra., 93, 397–413, 2005.

Moody, E. G., King, M. D., Platnick, S., Schaaf, C. B., and Gao, F.: Spatially complete global spectral surface albedos: value-added datasets derived from Terra MODIS land products, IEEE T. Geosci. Remote, 43, 144–158, 2005.

ACPD
14, 8779–8818, 2014

ARF Iberian Peninsula

D. Mateos et al.

Navas-Guzmán, F., Bravo-Aranda, J. A., Guerrero-Rascado, J. L., Granados-Muñoz, M. J., and Alados-Arboledas, L.: Statistical analysis of aerosol optical properties retrieved by Raman lidar over Southeastern Spain, Tellus B, 65, 21234, doi:10.3402/tellusb.v65i0.21234, 2013.

Nikitidou, E., Kazantzidis, A., De Bock, V., and De Backer, H.: The aerosol forcing efficiency in the UV region and the estimation of single scattering albedo at a typical West European site, Atmos. Environ., 69, 313–320, doi:10.1016/j.atmosenv.2012.12.035, 2013.

Obregón, M. A., Pereira, S., Wagner, F., Serrano, A., Cancillo, M. L., and Silva, A. M.: Regional differences of column aerosol parameters in western Iberian Península, Atmos. Environ., 62, 208–219, doi:10.1016/j.atmosenv.2012.08.016, 2012.

Pace, G., di Sarra, A., Meloni, D., Piacentino, S., and Chamard, P.: Aerosol optical properties at Lampedusa (Central Mediterranean). 1. Influence of transport and identification of different aerosol types, Atmos. Chem. Phys., 6, 697–713, doi:10.5194/acp-6-697-2006, 2006.

Panicker, A. S., Pandithurai, G., Safai, P. D., and Kewat, S.: Observations of enhanced aerosol longwave radiative forcing over an urban environment, Geophys. Res. Lett., 35, L04817, doi:10.1029/2007GL032879, 2008.

Penner, J. E., Andreae, M., Annegarn, H., Barrie, L., Feichter, J., Hegg, D., Jayaraman, A., Leaitch, R., Murphy, D., Nganga, J., Pitari, G., Ackerman, A., Adams, P., Austin, P., Boers, R., Boucher, O., Chin, M., Chuang, C., Collins, B., Cooke, W., DeMott, P., Feng, Y., Fischer, H., Fung, I., Ghan, S., Ginoux, P., Gong, S. L., Guenther, A., Herzog, M., Higurashi, A., Kaufman, Y., Kettle, A., Kiehl, J., Koch, D., Lammel, G., Land, C., Lohmann, U., Madronich, S., Mancini, E., Mischenko, M., Nakajima, T., Quinn, P., Rasch, P., Roberts, D. L., Savoie, D., Schwartz, S., Seinfeld, J., Soden, B., Tanré, D., Taylor, K., Tegen, I., Tie, X., Vali, G., Van Dingenen, R., van Weele, M., and Zhang, Y.: Aerosols, their direct and indirect effects, in: Climate Change 2001: the Scientific Basis, Report to Intergovernmental Panel on Climate Change from the Scientific Assessment Working Group (WGI), edited by: Houghton, J. T., Ding, Y., Griggs, D. J., Noguer, M., Van der Linden, P. J., Dai, X., Maskell, K., and Johnson, C. A., Cambridge University Press, Cambridge, UK and New York, NY, USA„ 289–416, 2001.

Pérez-Ramírez, D., Aceituno, J., Ruiz, B., Olmo, F. J., and Alados-Arboledas, L.: Development and calibration of a star photometer to measure the aerosol optical depth: smoke observations at a high mountain site, Atmos. Environ., 42, 2733–2738, 2008.

Pey, J., Querol, X., Alastuey, A., Forastiere, F., and Stafoggia, M.: African dust outbreaks over the Mediterranean Basin during 2001–2011: PM_{10} concentrations, phenomenology and

trends, and its relation with synoptic and mesoscale meteorology, Atmos. Chem. Phys., 13, 1395–1410, doi:10.5194/acp-13-1395-2013, 2013.
Prats, N., Cachorro, V. E., Berjón, A., Toledano, C., and De Frutos, A. M.: Column-integrated aerosol microphysical properties from AERONET Sun photometer over southwestern Spain, Atmos. Chem. Phys., 11, 12535–12547, doi:10.5194/acp-11-12535-2011, 2011.
Rajeev, K. and Ramanathan, V.: Direct observations of clear-sky aerosol radiative forcing from space during the Indian Ocean Experiment, J. Geophys. Res., 106, 17221–17235, doi:10.1029/2000JD900723, 2001.
Reche, C., Viana, M., Moreno, T., Querol, X., Alastuey, A., Pey, J., Pandolfi, M., Prévôt, A., Mohr, C., Richard, A., Artiñano, B., Gomez-Moreno, F. J., and Cots, N.: Peculiarities in atmospheric particle number and size-resolved speciation in an urban area in the western Mediterranean: results from the DAURE campaign, Atmos. Environ., 45, 5282–5293, doi:10.1016/j.atmosenv.2011.06.059, 2011.
Román, R., Antón, M., Valenzuela, A., Gil, J. E., Lyamani, H., de Miguel, A., Olmo, F. J., Bilbao, J., and Alados-Arboledas, L.: Evaluation of the desert dust effects on global, direct, and diffuse spectral ultraviolet irradiance, Tellus B, 65, 19578, doi:10.3402/tellusb.v65i0.19578, 2013.
Ruckstuhl, C., Philipona, R., Behrens, K., Coen, M. C., Dürr, B., Heimo, A., Mätzler, C., Nyieki, S., Ohmura, A., Vuilleumier, L., Weller, M., Wehrli, C., and Zelenka, A.: Aerosol and cloud effects on solar brightening and the recent rapid warming, Geophys. Res. Lett., 35, L12708, doi:10.1029/2008GL034228, 2008.
Saha, A., Mallet, M., Roger, J. C., Dubuisson, P., Piazzola, J., and Despiau, S.: One year measurements of aerosol optical properties over an urban coastal site: effect on local direct radiative forcing, Atmos. Res., 90, 195–202, doi:10.1016/j.atmosres.2008.02.003, 2008.
Sanchez-Lorenzo, A., Calbó, J., and Wild, M.: Global and diffuse solar radiation in Spain: building a homogeneous dataset and assessing trends, Global Planet. Change, 100, 343–352, doi:10.1016/j.gloplacha.2012.11.010, 2013.
Santos, D., Costa, M. J., and Silva, A. M.: Direct SW aerosol radiative forcing over Portugal, Atmos. Chem. Phys., 8, 5771–5786, doi:10.5194/acp-8-5771-2008, 2008.
Schuster, G. L., Dubovik, O., and Holben, B. N.: Angstrom exponent and bimodal aerosol size distributions, J. Geophys. Res., 111, D07207, doi:10.1029/2005JD006328, 2006.
Stamnes, K., Tsay, S. C., Wiscombe, W., and Laszlo, I.: DISORT, a General-Purpose Fortran Program for Discrete-Ordinate-Method Radiative Transfer in Scattering and Emitting Lay-

ACPD
14, 8779–8818, 2014

ered Media: Documentation of Methodology, Tech. rep., Dept. of Physics and Engineering Physics, Stevens Institute of Technology, Hoboken, NJ 07030, 2000.

Toledano, C., Cachorro, V. E., Berjon, A., de Frutos, A. M., Sorribas, M., de la Morena, B., and Goloub, P.: Aerosol optical depth and Ångström exponent climatology at El Arenosillo AERONET site (Huelva, Spain), Q. J. Roy. Meter. Soc., 133, 795–807, 2007a.

Toledano, C., Cachorro, V. E., de Frutos, A. M., Sorribas, M., Prats, N., and de la Morena, B.: Inventory of African desert dust events over the southwestern Iberian Peninsula in 2000–2005 with an AERONET Cimel Sun photometer, J. Geophys. Res., 112, D21201, doi:10.1029/2006JD008307, 2007b.

Valenzuela, A., Olmo, F. J., Lyamani, H., Antón, M., Quirantes, A., and Alados-Arboledas, L.: Aerosol radiative forcing during African desert dust events (2005–2010) over Southeastern Spain, Atmos. Chem. Phys., 12, 10331–10351, doi:10.5194/acp-12-10331-2012, 2012.

Zhou, M., Yu, H., Dickinson, R. E., Dubovik, O., and Holben, B. N.: A normalized description of the direct effect of key aerosol types on solar radiation as estimated from Aerosol Robotic Network aerosols and Moderate Resolution Imaging Spectroradiometer albedos, J. Geophys. Res., 110, D19202, doi:10.1029/2005JD005909, 2005.

Table 1. Coordinates and time interval of the six AERONET sites used in this study.

Station	Latitude (° N)	Longitude (° E)	Altitude a.s.l. (m)	Time interval
Palencia	41.99	−4.52	750	2003–2011
Barcelona	41.39	2.12	125	2004–2012
Cabo da Roca	38.78	−9.50	140	2003–2011
Évora	38.57	−7.91	293	2005–2012
Granada	37.16	−3.61	680	2004–2012
El Arenosillo	37.11	−6.73	0	2000–2009

ACPD
14, 8779–8818, 2014

Table 2. Summary of AERONET data used for ARE calculations: aerosol optical depth (AOD), single scattering albedo (SSA), asymmetry factor (g), precipitable water vapor column (PWC). Estimated absolute uncertainty of AOD and SSA is given according to Dubovik et al. (2002), and PWC error from Holben et al. (1998).

	AERONET database	Estimated uncertainty
AOD	Level 2.0	±0.01–0.02
SSA, g ($AOD_{440} > 0.4$)	Level 2.0	±0.03 (in SSA)
SSA, g ($0.15 < AOD_{440} < 0.4$)	Level 1.5-filtered*	±0.05–0.07(in SSA)
SSA, g ($AOD_{440} < 0.15$)	Fixed value	
PWC	Level 2.0	10–15 %

*Filters applied are the same as in level 2.0 except for AOD_{440} (see text).

Table 3. AFE values and their standard error for the UV, VIS, NIR, and SW ranges for, separately, four SSA and three α intervals over the Iberian Peninsula. Units are $\text{W m}^{-2}\tau^{-1}$. SSA groups: $0.85 \geq \text{SSA}_1 > 0.80$ (group 1), $0.90 \geq \text{SSA}_2 > 0.85$ (group 2), $0.95 \geq \text{SSA}_3 > 0.90$ (group 3), and $1.0 \geq \text{SSA}_4 > 0.95$ (group 4); and α groups: $0 \leq \alpha_1 \leq 1$ (group 1), $1.0 \leq \alpha_2 \leq 1.5$ (group 2), and $1.5 < \alpha_3 \leq 2$ (group 3). The average values without any classification are also presented.

Variable	Group	AFE_{UV}	AFE_{VIS}	AFE_{NIR}	AFE_{SW}
α	1	-5.41 ± 0.06	-30.1 ± 0.3	-20.9 ± 0.2	-56.5 ± 0.5
	2	-6.60 ± 0.09	-38.3 ± 0.4	-19.1 ± 0.2	-64.0 ± 0.6
	3	-7.06 ± 0.10	-39.4 ± 0.4	-16.9 ± 0.2	-63.3 ± 0.7
SSA	1	-9.7 ± 0.2	-52.8 ± 0.8	-24.9 ± 0.5	-87.4 ± 1.4
	2	-8.19 ± 0.10	-44.6 ± 0.4	-21.2 ± 0.2	-74.0 ± 0.6
	3	-6.37 ± 0.05	-35.9 ± 0.2	-19.5 ± 0.2	-61.8 ± 0.3
	4	-4.59 ± 0.05	-26.6 ± 0.2	-18.1 ± 0.2	-49.3 ± 0.3
Average		-5.98 ± 0.05	-33.7 ± 0.2	-19.34 ± 0.11	-59.1 ± 0.3

ACPD
14, 8779–8818, 2014

ARF Iberian Peninsula

D. Mateos et al.

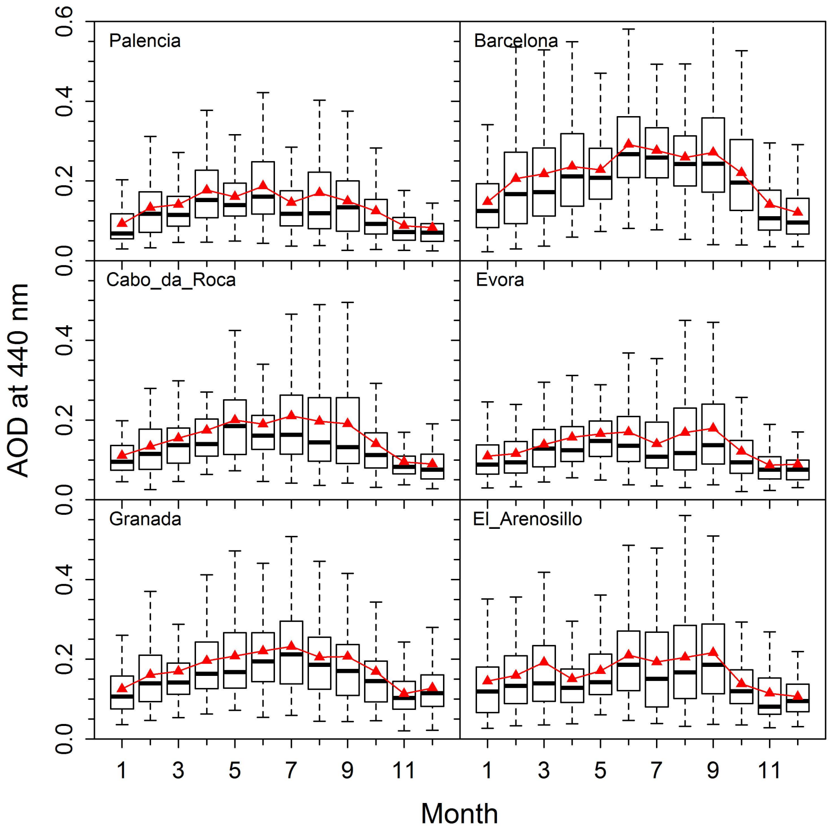

Fig. 1. Annual cycle of daily values of AOD at 440 nm by box whisker plots. Triangles and horizontal solid lines indicate the monthly average and median values, respectively.

ACPD
14, 8779–8818, 2014

ARF Iberian Peninsula

D. Mateos et al.

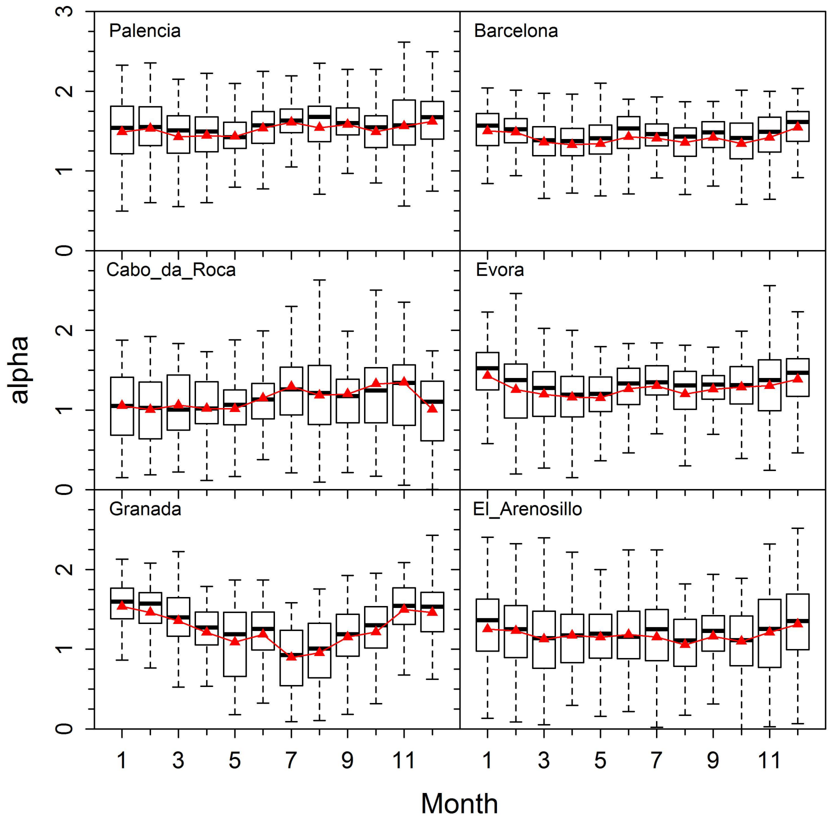

Fig. 2. Annual cycle of daily values of α ("alpha" in the figure) by box whisker plots. Triangles and horizontal solid lines indicate the monthly average and median values, respectively.

ACPD
14, 8779–8818, 2014

Title Page
Abstract | Introduction
Conclusions | References
Tables | Figures
◀| |▶
◀ ▶
Back | Close
Full Screen / Esc
Printer-friendly Version
Interactive Discussion

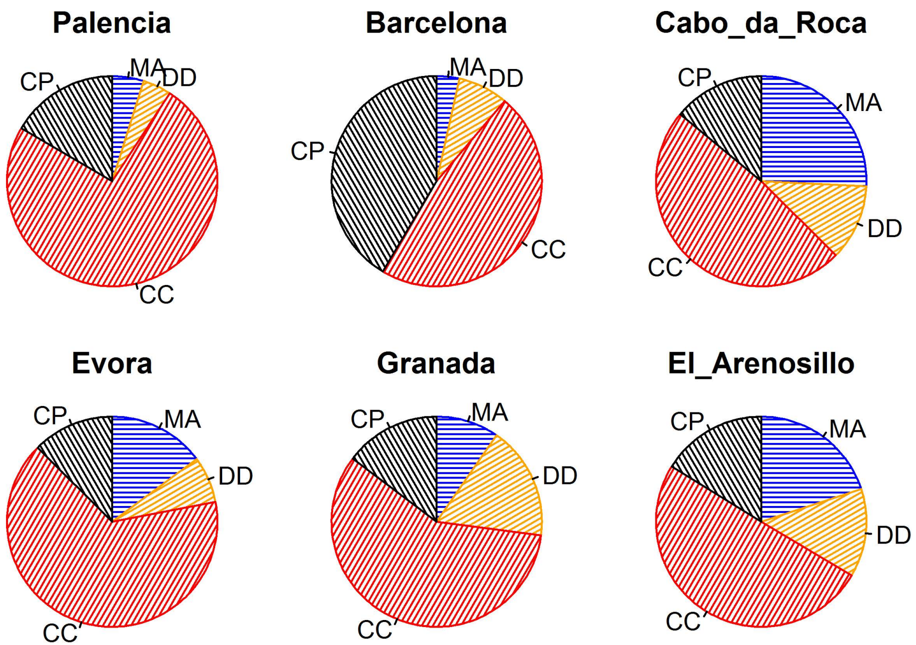

Fig. 3. Relative frequency of aerosol type occurrence: maritime (MA), desert dust (DD), continental clean (CC), and continental polluted (CP).

ACPD
14, 8779–8818, 2014

ARF Iberian Peninsula

D. Mateos et al.

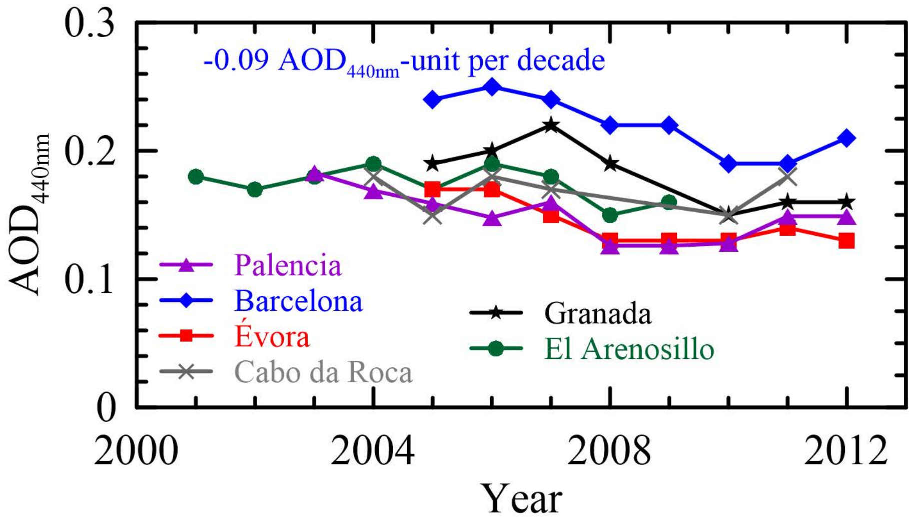

Fig. 4. Yearly values of $AOD_{440\,nm}$ at the six sites: Barcelona (blue diamonds), Palencia (purple triangles), Évora (red squares), Cabo da Roca (grey crosses), Granada (black stars), and El Arenosillo (green circles). The text points out the statistically significant trend obtained.

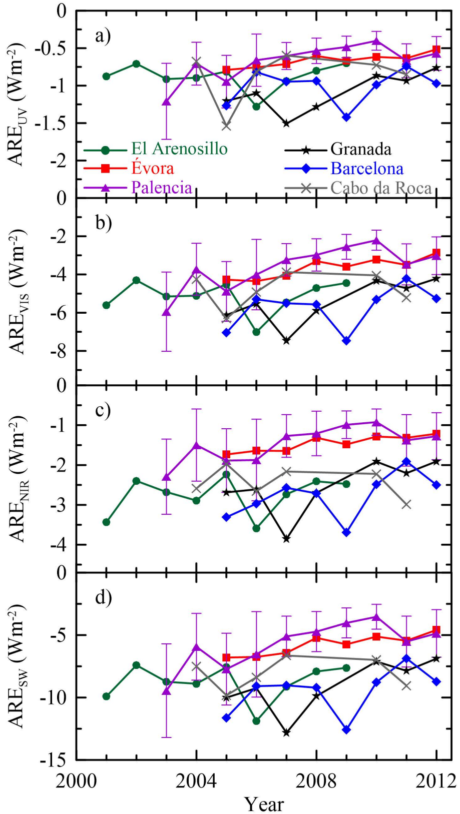

Fig. 5. Evolution of yearly ARE_{UV} **(a)**, ARE_{VIS} **(b)**, ARE_{NIR} **(c)**, and ARE_{SW} **(d)** at the six sites: Barcelona (blue diamonds), Palencia (purple triangles), Évora (red squares), Cabo da Roca (grey crosses), Granada (black stars), and El Arenosillo (green circles). Vertical bars indicate the standard deviation of each yearly value at Palencia station.

ACPD
14, 8779–8818, 2014

ARF Iberian Peninsula

D. Mateos et al.

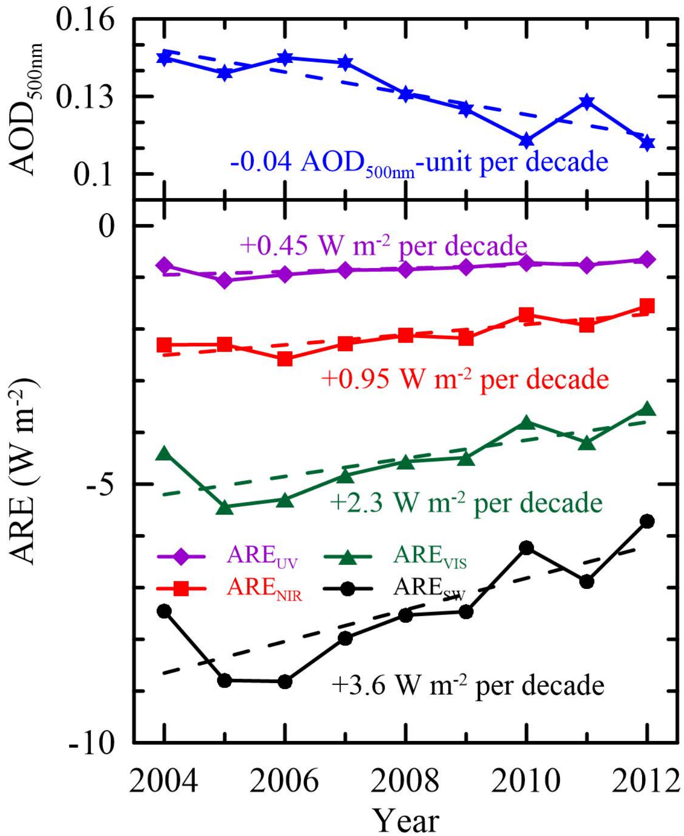

Fig. 6. Evolution of annual ARE at the four spectral ranges (ARE_{UV} purple diamonds, ARE_{VIS} red squares, ARE_{NIR} green triangles, and ARE_{SW} black circles) and AOD at 500 nm (blue stars) averaging the data from the six Iberian ground-based sites (only years with at least three sites considered). Dashed lines point out the linear trends (see text).

ACPD
14, 8779–8818, 2014

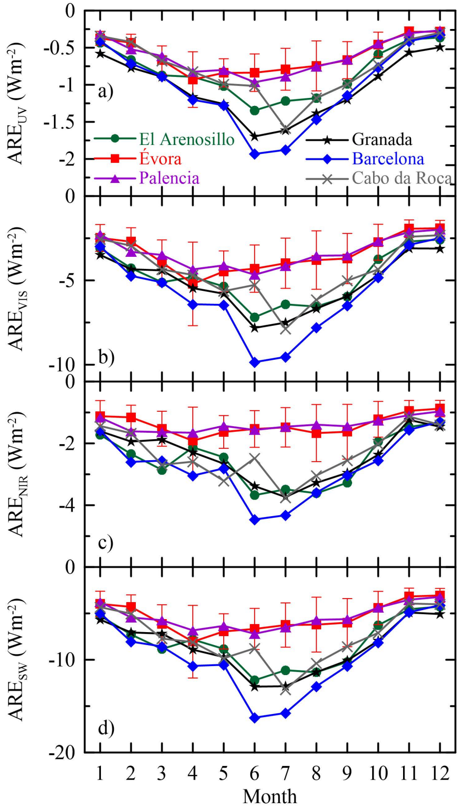

Fig. 7. Annual cycle of ARE_{UV} **(a)**, ARE_{VIS} **(b)**, ARE_{NIR} **(c)**, and ARE_{SW} **(d)** at the six sites: Barcelona (blue diamonds), Palencia (purple triangles), Évora (red squares), Cabo da Roca (grey crosses), Granada (black stars), and El Arenosillo (green circles). Vertical bars point out the standard deviation of each monthly value at Évora station.

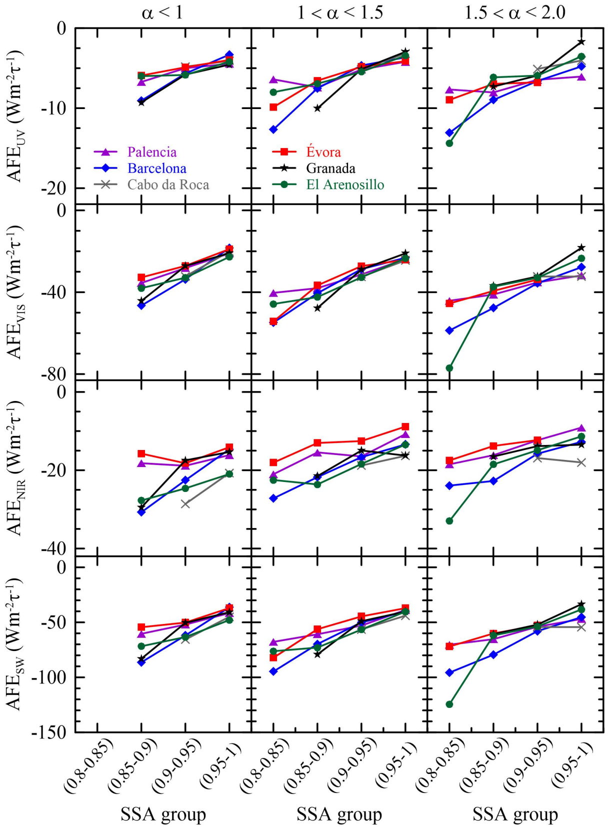

Fig. 8. AFE_{UV}, AFE_{VIS}, AFE_{NIR}, and AFE_{SW} against four groups of aerosol single scattering albedo and three intervals of α at the six sites: Barcelona (blue diamonds), Palencia (purple triangles), Évora (red squares), Cabo da Roca (grey crosses), Granada (black stars), and El Arenosillo (green circles).

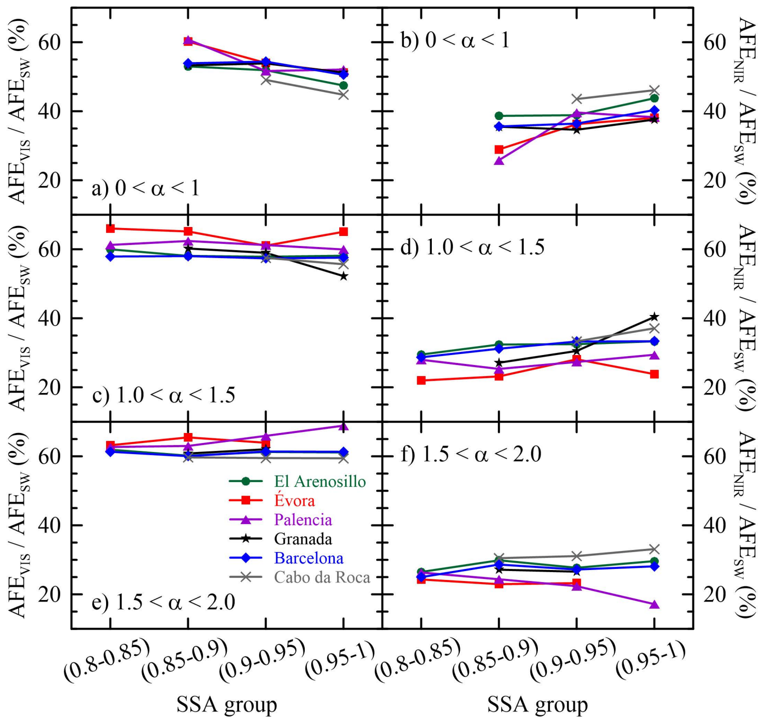

Fig. 9. Dependence of AFE_{VIS}/AFE_{SW} **(a, c, e)** and AFE_{NIR}/AFE_{SW} **(b, d, f)** ratios on SSA for large **(a, b)**, medium **(c, d)** and small **(e, f)** particles at the six sites: Barcelona (blue diamonds), Palencia (purple triangles), Évora (red squares), Cabo da Roca (grey crosses), Granada (black stars), and El Arenosillo (green circles).